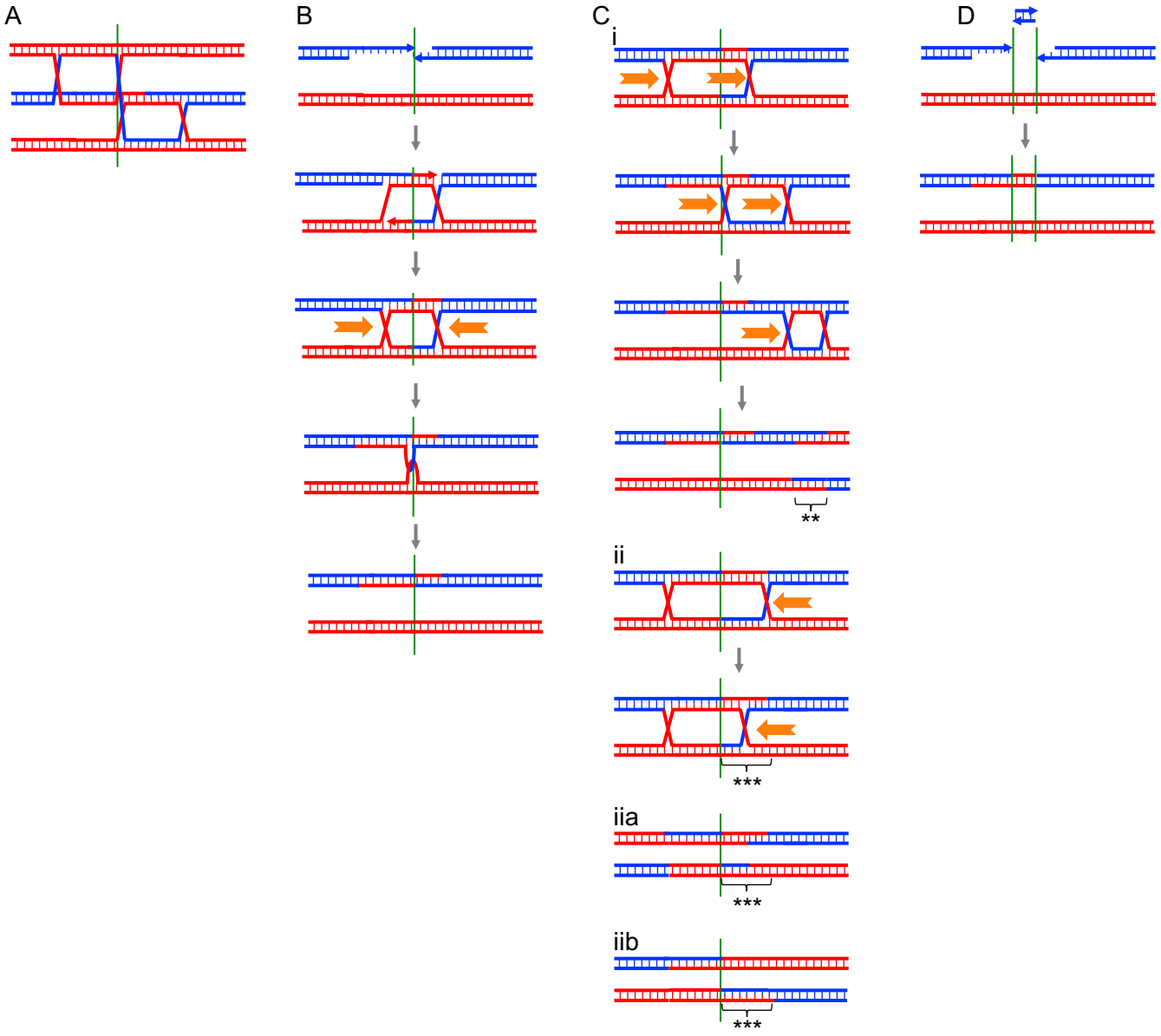

Figure S1 – Other recombination mechanisms and intermediates, related to Figure 1.
(A) An example of multi-chromatid joint molecule in which a single DSB can engage more than one repair template and create hybrid DNA on three or more chromatids.
(B) dHJ dissolution (Wu and Hickson, 2003). Helicase-driven inward migration of the two Holliday junctions (orange arrows) followed by single-strand decatenation produces an NCO with hybrid DNA on both sides of the DSB.
C) Holliday junction branch migration. Holliday junction movement, by breaking old base-pairs and making new ones, can lead to dHJ migration to a new position. i) Movement of both junctions can result in crossovers with symmetrical hybrid DNA (**) that are separated from the DSB by parental DNA. Note that the hybrid DNA tract associated with the DSB is flanked by parental sequences in a noncrossover configuration. ii) Movement of one junction can produce hybrid DNA tracts that switch between parental molecules (***) at a point away from the DSB; resolution as a crossover produces either a hybrid DNA tract switch remote from the DSB (iia) or a canonical DSBR product (iib).
(D) Multiple DSBs on a single chromatid produce a double-strand gap, which when repaired contains a patch of full conversion (6:2 segregation) in between the two DSBs.

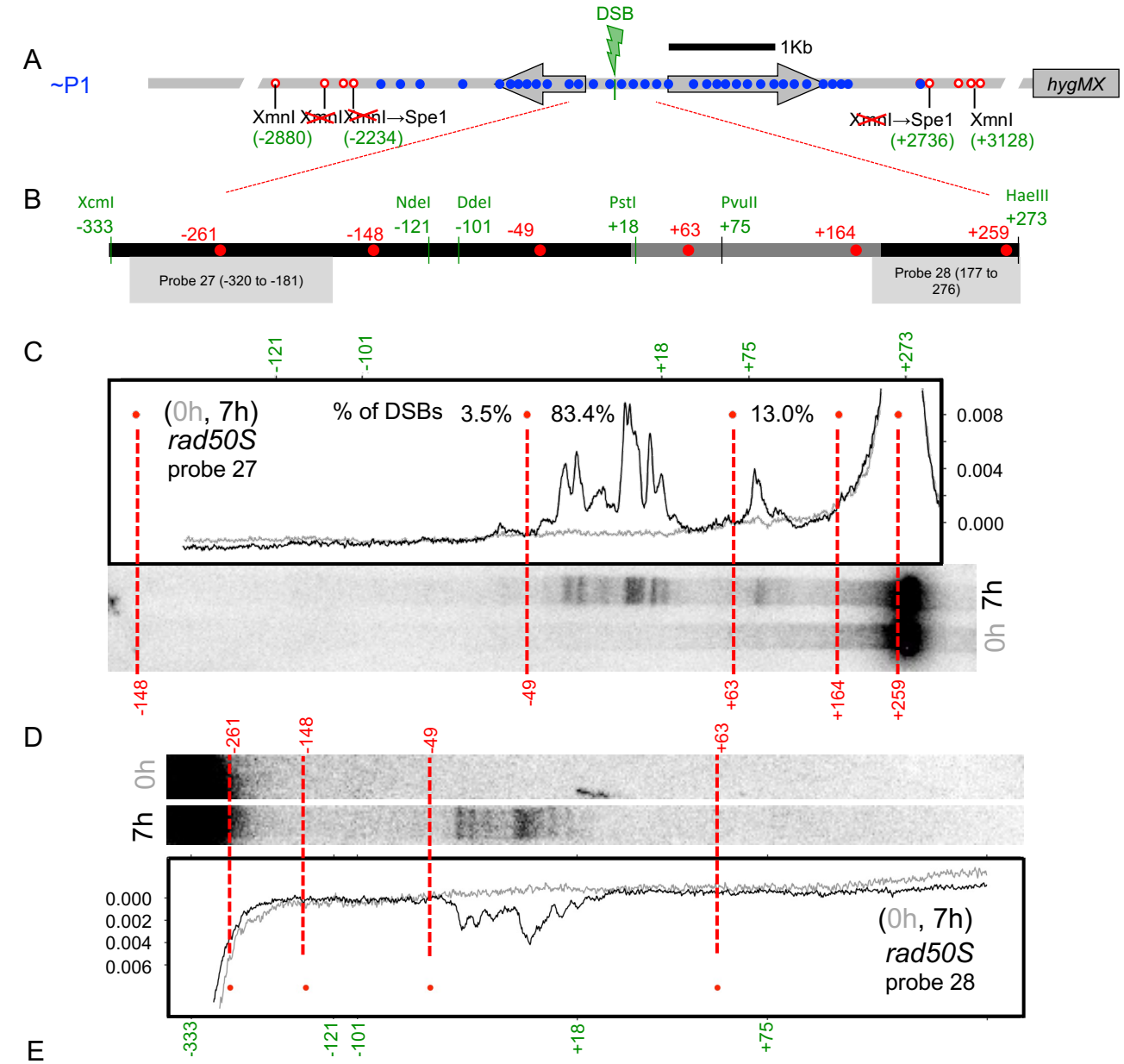

side	K ± S.E.	processivity
left	$9.6\times10^{-4} \pm 0.3\times10^{-4}$	0.9990
right	$8.5\times10^{-4} \pm 0.1\times10^{-4}$	0.9991
all	$8.9\times10^{-4} \pm 0.2\times10^{-4}$	0.9991

Figure S2. Fine-structure DSB maps and conversion tract analysis, related to Figure 2.

(A) Illustration of parent ~P1, which lacks SNPs between nt -2236 and +2736, but contains flanking XmnI site polymorphisms to allow for scoring recombination on Southern blots.

(B) Hotspot region (-333 to +273) used for high resolution DSB analysis. Green–restriction sites used for size standards; red–polymorphic marker (SNP) positions.

(C, D) Blots of polyacrylamide gels with rad50S samples digested with XcmI and HaeIII and probed with probes 27 and 28, respectively, with plots of lane signal intensity. Full gel images available at doi:10.17632/j2jpj3p29f.1

(E) Gene conversion half-tract lengths (distance from DSB to most distal converted marker) were fitted to an exponential decay curve. Two-sided events were disaggregated into left-hand and right-hand half-tracts. Processivity—fraction of tracts ≥ n nt that are ≥ n+1 nt, calculated as described (de Massy, 2003).

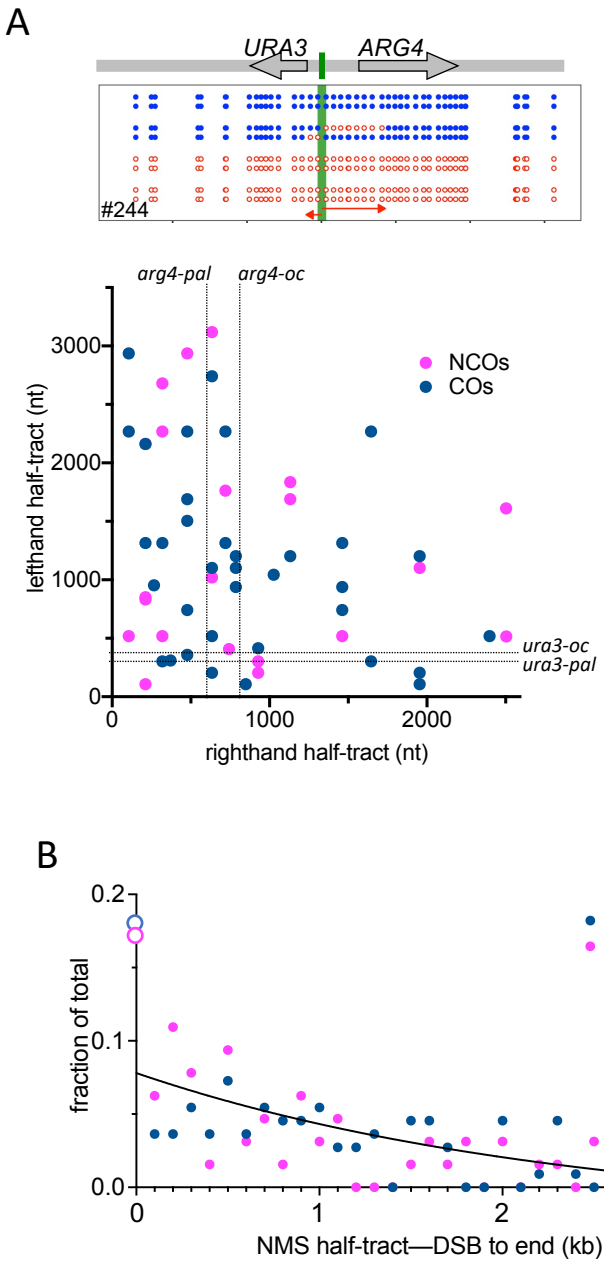

Figure S3. Further conversion tract analysis, related to Figure 3.
(A) Independent end extension in two-sided events. Top—two-sided NCO illustrating left-hand (leftward arrow) and right-hand (rightward arrow) half-tracts. Bottom—half-tract lengths in two-sided COs (blue) and NCOs (magenta) are plotted. Left-hand and right-hand tracts in the same event are poorly correlated (Spearman rank-order correlation, p=0.09, r=-0.2). Dotted lines denote location of arg4 and ura3 loss of function mutations used in conventional tetrad analysis in this study (Figure 2C and Supplementary Table 1.5; arg4-oc and ura3-oc) and in Jessop et al. (2005; arg4-pal and ura3-pal). Two-sided events detected by SNP analysis to the left of or below these lines would have been scored as one-sided had conventional marker analysis been used.
(B) Non-cumulative distribution of NMS half-tract lengths, partitioned in 0.1 kb bins. Black line–exponential decay curve fitted to non-zero values. Open-circles—"invisible" half-tracts (<100nt), assuming that one-sided events contain a second "invisible" half-tract.

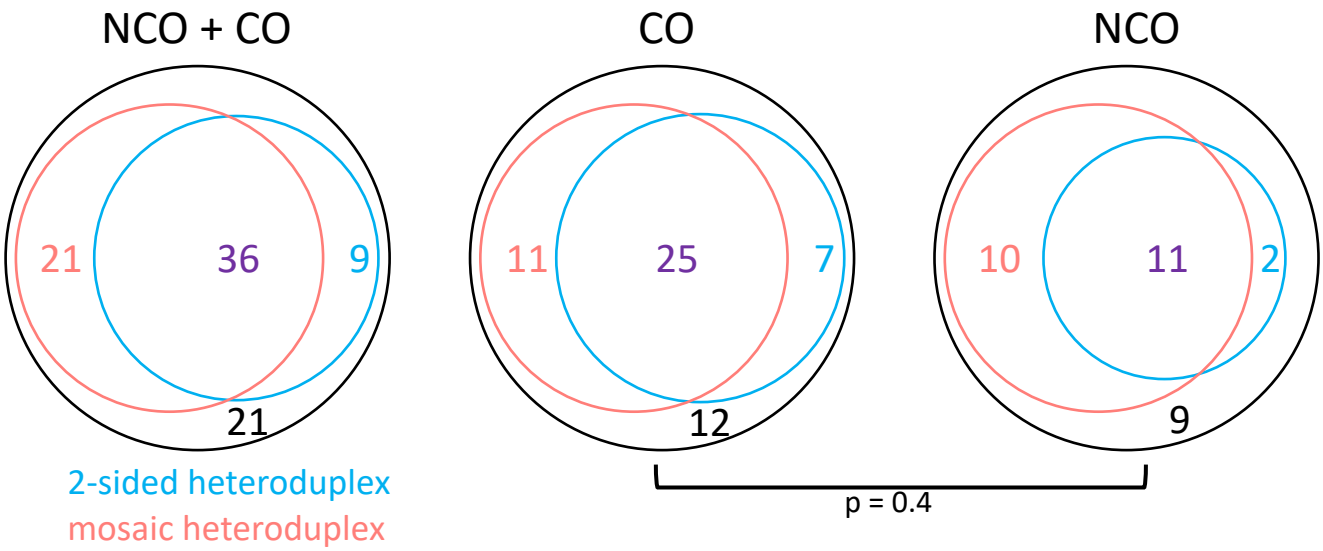

Figure S4. Multiple end invasions are common in both COs and NCOs, related to Figures 3 and 4.
Venn diagrams showing number of events with 2-sided heteroduplex (both DSB ends invade; cyan), mosaic heteroduplex (template switching; coral), or both (purple). Black—one-sided events with continuous heteroduplex (no template switching). Five crossover tetrads were too complex to score unambiguously. The distributions of events in NCOs and COs are not significantly different (chi-square test).

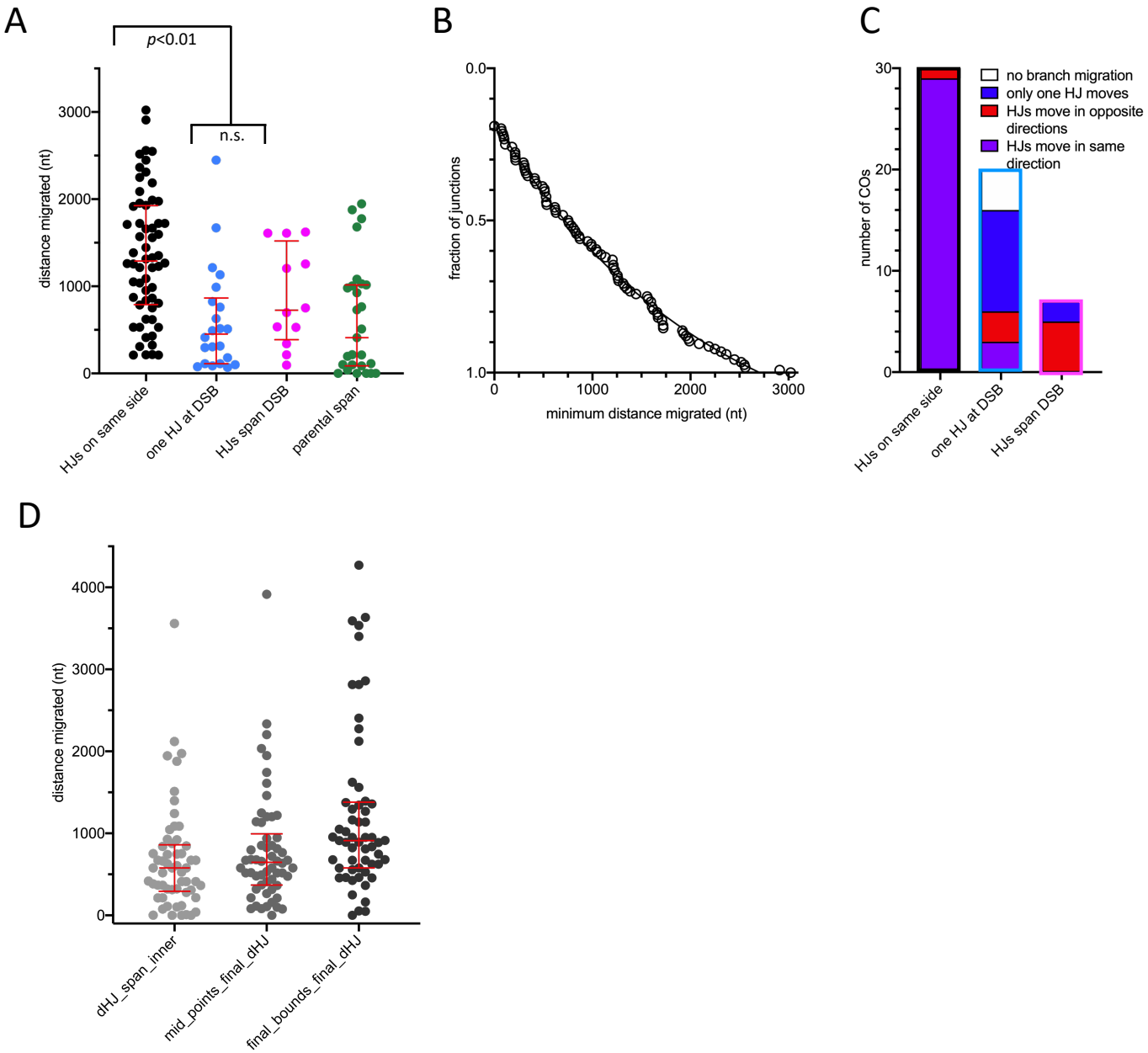

Figure S5. Properties of branch migration, related to Figure 5.

A) Branch migration distances for each of the two Holliday junctions in COs, calculated by subtracting inferred initial junction positions from inferred final junction positions (see Figure 5A for examples). Black—final positions of both junctions are on one side of the DSB; turquoise—one junction is not separated from the DSB; pink—the two junctions are on opposite sides of the DSB (pink); green—extent of intervening parental sequences separating initial and final dHJ positions (see Figure 5A). Red bars denote median and quartiles. p values are from Mann Whitney rank tests.

(B) rank order plot of distance each individual Holliday junction has branch migrated, including 10 junctions where migration was not detected. The curve is an exponential decay with a half-distance of 1kb, r2 = 0.99.

(C) Types of branch migration for each class of crossovers.

(D) Distance between final Holliday junctions; junction positions calculated relative to the two markers flanking the junction as follows: minimum—at the inner pair of flanking markers; midpoint—halfway between the flanking markers; maximum—at the outer pair of flanking markers. Red bars denote median and 1st and 3rd quartiles.

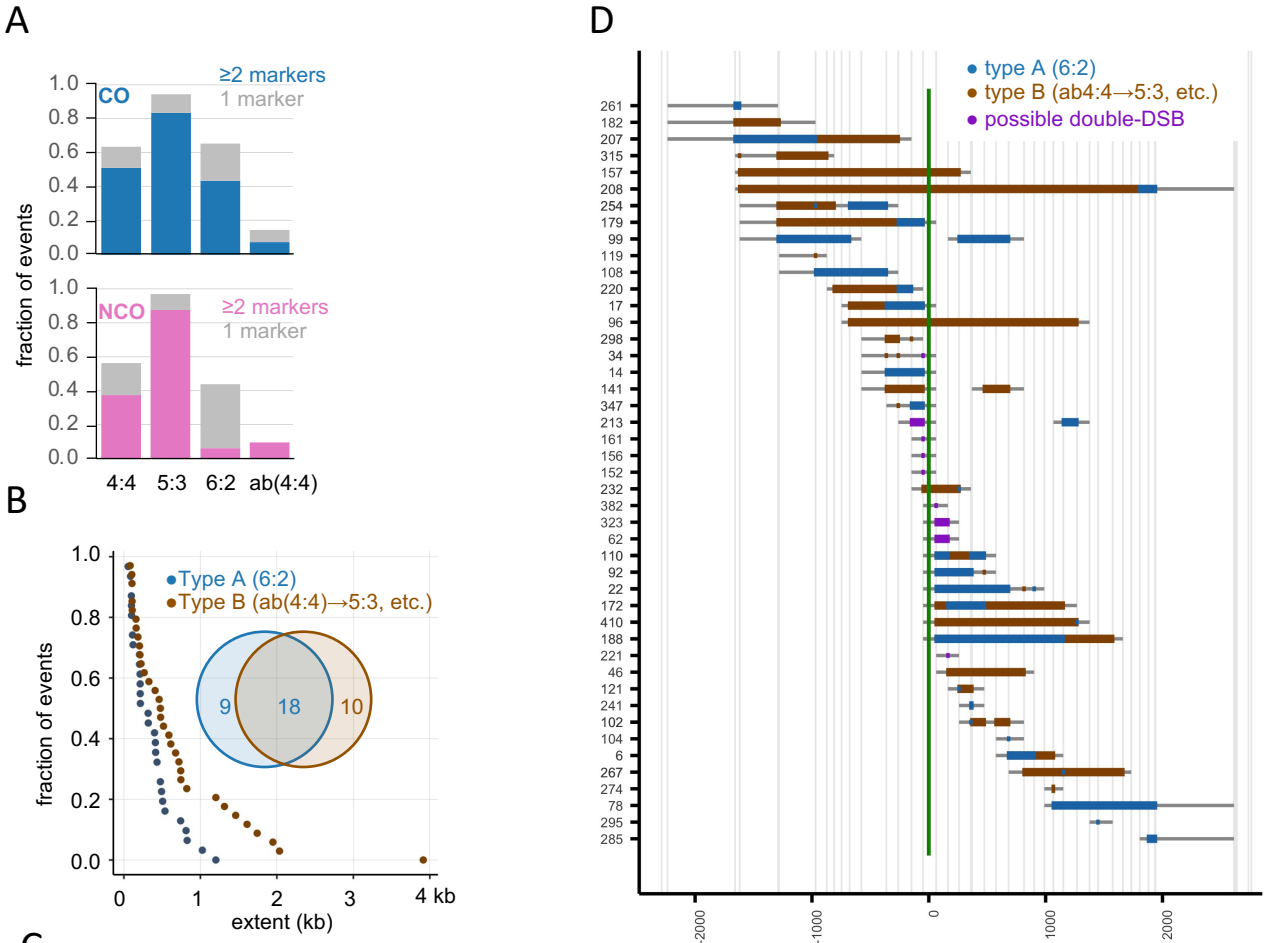

C

Strand processing segment lengths

Excluding single-marker segments	mean± std.dev	# segments	# tetrads
Type A (6:2)	498 ± 278	21	19
Type B (ab(4:4)→5:3, etc.)	947 ± 834	25	22
Including single-marker segments			
Type A (6:2)	372 ± 294	31	27
Type B (ab(4:4)→5:3, etc.)	730 ± 800	34	28

Figure S6. Strand processing signatures among crossovers, related to Figure 6.
A) abundance of various marker segregation types among tetrads in the crossover and the noncrossover categories.
(B) Rank order plots of strand processing tract lengths, including single-marker tracts. Median tract lengths: type A—316 nt; type B— 478 nt. Inset—Venn diagram showing number of tetrads with Type A, Type B, and both types of processing if single marker events are included.
(C) Other features of strand processing segments.
(D) Map of all strand processing events. Vertical lines—marker locations. Solid bars–markers included in each event; grey horizontal lines—maximum extent of each event. Dots—single marker events; these were not included in most calculations. 6:2 segregations that might reasonably be produced by a double DSB are indicated in purple.

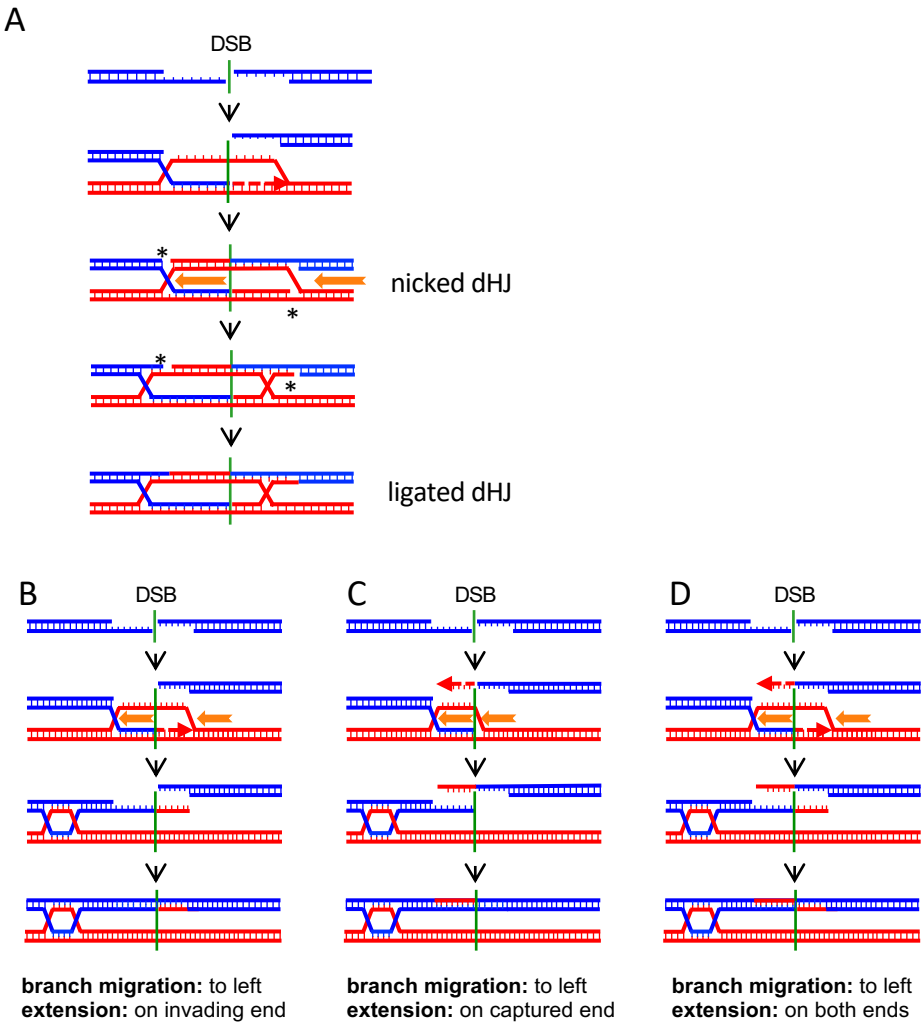

Figure S7 – Different branch migration and annealing regimes, related to Figure 7.
A) In the canonical DSBR model, where annealing immediately follows invasion and extension (Szostak et al., 1983), branch migration (orange arrows) for a short distance is required to move strand discontinuities at each branch (asterisks) into duplex DNA, where they can be ligated.
B) Branch migration as in Figure 7. Synthesis from the invading end, followed by branch migration and annealing with an unextended DSB end, produces a crossover and hybrid DNA on opposite sides of the DSB.
C) Invasion without synthesis, followed by branch migration and annealing with an extended DSB end, produces a CO and hybrid DNA on the same side of the DSB.
D) Synthesis from the invading end, followed by branch migration and annealing with an extended DSB end, produces a CO with hybrid DNA on both sides of the DSB.